Heliyon 10 (2024) e36570

Contents lists available at ScienceDirect

Heliyon

journal homepage: www.cell.com/heliyon

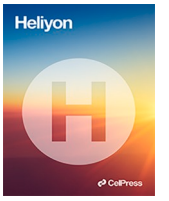

Research article

PGRMC2 influences the onset of postmenopausal osteoporosis through disulfidptosis in monocytes: Evidence from experimental validation and Mendelian randomization

Yaobin Wang [a,b,c,d,1], Hefang Xiao [a,b,c,1], Yi Chen [a,b,c], Xiaoyun Sheng [a,b,c], Zhiwei Feng [a,b,c], Bo Peng [a,b,c], Zhongcheng Liu [a,b,c], Hongwei Zhan [a,b,c], Dejian Xiang [a,b,c], Chengjun Zhang [a,b,c], Yayi Xia [a,b,c,*], Bin Geng [a,b,c,**]

[a] *Department of Orthopaedics, Lanzhou University Second Hospital, Lanzhou, Gansu, 730030, China*
[b] *Orthopaedic Clinical Research Center of Gansu Province, Lanzhou, Gansu, 730030, China*
[c] *Intelligent Orthopaedic Industry Technology Center of Gansu Province, Lanzhou, Gansu, 730030, China*
[d] *Second Department of Orthopedics, The Fifth Affiliated Hospital of Zhengzhou University, Zhengzhou, Henan, 450000, China*

ARTICLE INFO

Keywords:
Disulfidptosis
PMOP
scRNA-seq
Microarray-based assay
Monocytes
Mendelian randomization

ABSTRACT

This study explores the role of disulfidptosis in monocytes and its relation to postmenopausal osteoporosis (PMOP). Using single-cell RNA sequencing and microarray assays, we identified key genes: LONRF1, ACAP2, IPO9, and PGRMC2. Through differential analysis, Weighted Gene Co-expression Network Analysis (WGCNA), and machine learning, these genes were linked to PMOP. Functional enrichment and ROC curve analysis demonstrated their effectiveness in distinguishing postmenopausal fracture patients from healthy individuals. Notably, PGRMC2 exhibited significant expression differences, highlighted by a notable Area Under the Curve (AUC) value of 0.665. Further investigation involved Western blotting and immunohistochemical assays, revealing decreased PGRMC2 expression in ovariectomized (OVX) mice. This decrease was consistent across both experimental methods, emphasizing PGRMC2's role in PMOP. Moreover, PGRMC2 was predominantly present in macrophages compared to monocytes within bone tissue and was significantly located in bone marrow mesenchymal stem cells (BM-MSCs) in PMOP patients. It was also abundantly found in osteoblasts and adipocytes. Additionally, a Mendelian randomization analysis using the TwoSampleMR R package, with data from decode and GWAS databases, was conducted. This analysis showed a significant impact of PGRMC2 on osteoporosis risk ($p = 0.0048$, $OR = 0.6836$), suggesting a potential protective effect against the disease. Our results suggest that PGRMC2 may facilitate the differentiation of monocytes into macrophages in bone tissue, influencing the behavior of BM-MSCs. This, in turn, could impact the progression and severity of PMOP. The study provides new insights into the molecular mechanisms underlying postmenopausal osteoporosis and highlights the potential of PGRMC2 as a therapeutic target or biomarker for this condition.

* Corresponding author. Department of Orthopaedics, Lanzhou University Second Hospital, Lanzhou, Gansu, 730030, China.
** Corresponding author. Department of Orthopaedics, Lanzhou University Second Hospital, Lanzhou, Gansu, 730030, China.
E-mail addresses: lanzhoux166@163.com (Y. Xia), 2025209545@qq.com (B. Geng).
[1] These authors contributed equally to this work.

https://doi.org/10.1016/j.heliyon.2024.e36570
Received 29 January 2024; Received in revised form 14 August 2024; Accepted 19 August 2024
Available online 19 August 2024

1. Introduction

Postmenopausal osteoporosis(PMOP) is a prevalent disease, particularly among women. This condition significantly impacts the quality of life for patients and increases the risk of fractures. According to research, 50 % of postmenopausal women will suffer from osteoporosis, with menopause being the most common cause [1]. In the United States, the number of women affected by osteoporosis is quite substantial. Based on the T-score for bone density, the prevalence of osteoporosis among postmenopausal women is 14 % in the age group of 50–59 years, 22 % in the 60–69 years age group, 39 % in the 70–79 years age group, and as high as 70 % in those aged 80 years and above [2]. In China, according to a systematic review, the prevalence of osteoporosis has been continuously increasing from 14.94 % in 2008 to 27.96 % between the years 2012 and 2015 [3]. Additionally, bone loss induced by menopause is closely related to the decline in estrogen levels. Prolonged low estrogen levels may lead to a further decrease in bone density. Postmenopausal osteoporosis is associated with reduced estrogen levels and is closely related to osteoclasts and osteoblasts. Dual-energy X-ray absorptiometry (DXA) can be used to measure bone density, helping to assess fracture risk and identify patients who may benefit from treatment [4]. In English and adhering to the language standards of a journal article: The first-line treatment for postmenopausal osteoporosis typically involves antiresorptive agents, such as bisphosphonates, which can slow down the rate of bone loss. Additionally, hormone therapy (HT) can help improve bone density and prevent osteoporosis. During treatment, patients may require calcium and vitamin D supplements or other fracture prevention measures [5]. Furthermore, non-pharmacological interventions, such as lifestyle changes, can also help manage postmenopausal osteoporosis [6]. However, many drugs have unknown complications, necessitating further exploration for more precise targeted diagnosis and treatment.

Single-cell analysis plays a critical role in disease research. With the emergence of single-cell studies in recent years, the resolution and scale of biological research have reached unprecedented levels [7]. In particular, single-cell analysis techniques, such as next-generation sequencing (NGS) and fluorescence-activated cell sorting (FACS), have helped reveal significant links between cell heterogeneity and disease progression. Moreover, omics analysis techniques can be used to identify key molecular mechanisms in an unbiased manner. Single-cell analysis techniques contribute to generating unprecedented maps of blood cells under healthy and diseased conditions [8]. By analyzing rich gene expression data at the single-cell level, we can gain insight into the nature of diseases [9].

Disulfidptosis is a previously unexplained type of cell death. This could open the door to new disease treatment strategies, according to this study. The study found that cells with higher levels of the SLC7A11 protein trigger disulfidptosis when subjected to glucose deprivation [10]. In cancer cells with aberrant expression of the cystine/glutamate transporter family member 7,11 (SLC7A11), there is a higher rate of cystine uptake and reduction to cysteine. When coupled with glucose deprivation, this leads to the accumulation of large amounts of intracellular disulfidptosis bond molecules and rapid cell death. This form of cell death is known as disulfidptosis. In a recent study, newly identified biomarkers associated with disulfidptosis were found to be useful for clinical diagnosis, prognosis prediction, and treatment targeting in liver cancer [11]. So far, the role of disulfidptosis in PMOP is not clear. The mechanism of disulfidptosis in this disease is worth further exploration and study. In this study, we used a combination of scRNA-seq and microarray-based assay to explore the potential mechanism of disulfidptosis in PMOP, and to identify diagnostic and therapeutic factors, as well as new approaches and methods for clinical immunotherapy planning and patient management.

2. Materials and methods

2.1. Data and sample sources

Microarray-based assay data GSE56815 was selected from the GEO database, which included 40 normal samples and 40 disease samples. Single-cell data GSE169396 was included, which contained 4 bone tissue samples, and GSE147287 was included, which contained 1 normal sample and 1 disease sample [12]. We collected samples from 12 patients, including 6 control and 6 disease samples from our hospital. The ethical batch number was 2023A-310, and peripheral blood mononuclear cells were collected for subsequent analysis.

2.2. Differential analysis

The limma package [13] was used for differential analysis of GSE56815, with a screening criterion of $p < 0.05$. The differentially expressed genes were selected for subsequent analysis.

2.3. WGCNA analysis

The WGCNA package [14] was used for WGCNA analysis of GSE56185, and the correlation between modules and disease status was analyzed. The parameters were power = 6, TOMType = "signed", minModuleSize = 30, reassignThreshold = 0, and mergeCutHeight = 0.25. The selected genes for further analysis had a standard deviation greater than zero, excluding abnormal data. The data was divided into different modules by identifying the module most positively associated with PMOP and setting the optimal soft threshold using the "pickSoftThreshold" function [15] of the "WGCNA" package with b = 19 as the power to establish an unscaled network. To merge similar modules in clusters, we set the threshold to 0.25, and the minimum number of modules was set to 30. Each module contained genes with similar co-expression characteristics.

2.4. Disulfidptosis-related genes

We obtained genes related to disulfidptosis from published literature and screened the top 200 key genes as the key genes for subsequent analysis [10]. In the references, the authors studied the induction process of disulfidptosis in disulfidptosis-related genes (such as SLC7A11) by measuring the levels of NADPH in cells under different conditions and assessing cell death under various conditions, thereby triggering cell death. This included genes that are directly involved in the process, as well as those that regulate or are regulated by disulfidptosis.

2.5. Intersection clustering analysis

The differentially expressed genes, WGCNA module genes, and disulfidptosis-related genes were intersected to determine the disulfidptosis-related genes that affect PMOP. These genes were used for clustering analysis using the ConsensusClusterPlus package. The clustering results were then analyzed using Single Sample Gene Set Enrichment Analysis (ssGSEA) [16], a method used to calculate the enrichment level of gene sets to evaluate the expression levels of gene sets in the samples.

2.6. Machine learning for further screening

The selected key genes were further screened using machine learning methods. Lasso screening was performed using the glmnet package [17], randomForest [18] screening was performed using the randomForest package, and SVM screening was performed using the e1071 package [19]. The top 6 genes from each method were selected and intersected to obtain the key genes for subsequent analysis.

2.7. Immune-related analysis

The CIBERSORT method [20] was used to analyze the immune cell infiltration levels between the disease and normal samples in GSE56185. The "PERM" parameter [21] was set to 1000 and the cutoff value was set at $p < 0.05$. In addition, the proportion of each immune cell type in the samples was calculated, and the pheatmap package [22,23] was used to create a heatmap of the 22 immune cells. The "corrplot" package [24,25] was used to create a correlation heatmap to visualize the correlations between the 22 different infiltrating immune cells. The Spearman rank correlation test in R was used to examine the relationship between the infiltrating immune cells and the final obtained gene biomarkers. The ggplot2 package was used for correlation analysis [26,27], and the pROC package was used for ROC curve validation [28,29].

2.8. Enrichment analysis

In this study, we performed enrichment analysis using Gene Set Variation Analysis (GSVA) and GSEA (Gene Set Enrichment Analysis) for four genes [30]. For the GSVA analysis, we used the gsva package with the parameters method = "gsva", kcdf = "Gaussian", mx.diff = FALSE, and verbose = FALSE. For the GSEA analysis, we used the clusterProfiler package with the parameters nPerm = 1000, minGSSize = 10, maxGSSize = 500, and pvalueCutoff = 0.05. In the GSEA analysis, we further annotated the results of the enrichment analysis.

2.9. Single-cell data analysis

We performed annotation analysis on datasets GSE169396 and GSE147287 using the Seurat method [31], and analyzed the distribution of key genes in cells using the Seurat package. Specific parameter settings were: min.cells = 3, min.features = 200, max.features = 2500, percent.mito = 0.05. We further filtered by setting cutoff values at 10 % for mitochondrial genes and 3 % for erythrocyte genes. After identifying 4000 highly variable genes for analysis, we adjusted the number of principal components (PCs) to different cell clusters and then displayed and annotated them using the "tSNE" plot [32]. Next, we annotated the datasets using the "FindAllmarkers" function in the Seurat R Package [33]. Finally, the "person" R package was used to plot the correlation analysis results

Table 1
qRT-PCR primer sequences.

GAPDH(F)	GCACCGTCAAGGCTGAGAAC
GAPDH(R)	TGGTGAAGACGCCAGTGGA
ACAP2(F)	CTTCAGCGGGTCCAGTGTATCC
ACAP2(R)	AGGTGATGCCCAGGTTGATGC
IPO9(F)	CCAGGAGGAGGAAGAGGAGGAG
IPO9(R)	CCTTCAGGGCATCAGGGTCATC
LONRF1(F)	CAGTTGAGGAAAGCGGTTTAGG
LONRF1(R)	TTCCAGATATTCAATGTCGGCAGTG
PGRMC2(F)	GCGGCAGCGAGAGTCCAG
PGRMC2(R)	GCAGCACCAGAGCCACCAG

of key genes, in order to explore the genes that are closely related to the key genes within the matrix. And we used the multiMiR package to predict the miRNAs related to the key genes.

2.10. Mendelian randomization

In this study, we employed the TwoSampleMR R package to perform Mendelian randomization analysis. Initially, we downloaded the information of PGRMC2 from the decode database and selected osteoporosis data from the GWAS database (code: finn-b-OSTEOPOROSIS_FRACTURE_FG). We then used the extract_outcome_data and harmonise_data functions from the TwoSampleMR package to extract the outcome data and harmonize the exposure and outcome data, respectively. Subsequently, we conducted Mendelian randomization analysis using the mr function, employing various methods (such as IVW, Egger regression, weighted median, etc.) to generate estimates and calculate the results for each method. To evaluate the robustness of the results, we performed a heterogeneity test by calculating the heterogeneity statistics using the mr_heterogeneity function. To assess whether the results could be influenced by confounding factors, we performed a pleiotropy test using the mr_pleiotropy_test function to calculate the pleiotropy statistics. Additionally, we conducted sensitivity analysis, including a leave-one-out analysis for each SNP, to assess whether the results might be affected by any particular SNP. Finally, we visualized the results of the Mendelian randomization analysis using the mr_scatter_plot, mr_forest_plot, mr_funnel_plot, and mr_leaveoneout functions.

2.11. Validation of key genes

Validation was performed using quantitative real-time PCR (qRT-PCR) [34]. Primer designs are listed in Table 1. Six normal samples and six control samples were analyzed to validate the key genes identified in this study. The 2ˆ-ΔΔCT method was used to calculate relative gene expression levels. The procedures are as follows:

Peripheral blood mononuclear cell (PBMC) isolation: Approximately 5–10 ml of blood was collected from patients, and PBMCs were isolated using the Ficoll gradient centrifugation method. Blood was mixed with an equal volume of PBS and carefully layered over Ficoll to avoid mixing. Centrifugation was performed at 400g for 30 min, and the rotor was stopped without using the brake. The PBMC layer (white layer at the interface between Ficoll and plasma) was collected and washed with PBS 2–3 times to remove residual Ficoll and plasma.

RNA extraction: Total RNA from PBMCs was extracted using TRIzol reagent. TRIzol was added to the cell lysate and mixed well. Chloroform was added for phase separation, and the aqueous phase was collected after centrifugation. An equal volume of isopropanol was added to precipitate RNA, and the supernatant was discarded after centrifugation. The RNA pellet was washed with 70 % ethanol, air-dried at room temperature, and dissolved in DEPC-treated water.

Reverse transcription: Total RNA was reverse transcribed into cDNA using a reverse transcription kit. Following the kit's instructions, RNA, random primers, dNTPs, reverse transcriptase, and buffer were mixed and subjected to the reaction. Reaction conditions were as follows: 25 °C for 10 min, 42 °C for 60 min, and 70 °C for 10 min to terminate the reaction.

qRT-PCR: SYBR Green qRT-PCR Master Mix was used for real-time quantitative PCR. Following the kit's instructions, cDNA, SYBR Green Master Mix, and forward and reverse primers were mixed, and qRT-PCR reaction conditions were set. Reaction conditions were as follows: initial denaturation at 95 °C for 10 min, followed by 40 cycles of denaturation at 95 °C for 15 s, annealing at 60 °C for 1 min, and a final melt curve analysis. β-actin was used as the reference gene.

Data analysis: Relative gene expression levels were calculated using the 2ˆ-ΔΔCT method. Calculation: ΔCT = CT (target gene) - CT (reference gene), ΔΔCT = ΔCT (disease group) - ΔCT (normal group), and the relative expression level was obtained by calculating 2ˆ-ΔΔCT. This method eliminates variations in experimental operation and RNA concentration, resulting in more accurate gene expression levels.

Statistical analysis: Compare the relative expression levels of key genes between the normal group and the control group. Use *t*-test to analyze the differences between the two groups.

2.12. Western blotting

Cells were lysed with RIPA lysis buffer (Beyotime, Shanghai, China) supplemented with protease inhibitor. The protein samples were extracted and quantified by BCA kit (Beyotime, Shanghai, China). The proteins were separated using sodium dodecyl sulfate-polyacrylamide gel electrophoresis and transferred onto polyvinylidene difluoride membranes (PVDF membranes). PVDF membranes were blocked with 5 % skim milk, and incubated at 4 °C in Anti-PGRMC2 (ab251875, 1:1000, Abcam) for 1 h at room time. They were detected with chemiluminescence system (Advansta, CA) and visualized by Bio-Rad ChemiDoc XRS + Imaging System (USA). Results were normalized to β-actin and quantified with ImageJ software.

2.13. Histological analysis

The paraffin-embedded discs were cut into 4 μm-thick sections. For histology, the sections were deparaffinized, rehydrated, and then stained with hematoxylin and eosin (HE) and Safranin O-Fast Green (SO). In addition, the histopathological grading scores were assessed according to the grading scale. For IHC staining, the sections were deparaffinized, rehydrated, and incubated with 3 % H2O2 for 20 min at room temperature to eliminate endogenous peroxidase activity. Then, the antigen was retrieved by pressure cooking in 10 mmol/L citrate buffer, pH = 6. Subsequently, the sections were blocked with 10 % goat serum albumin for 30 min at room

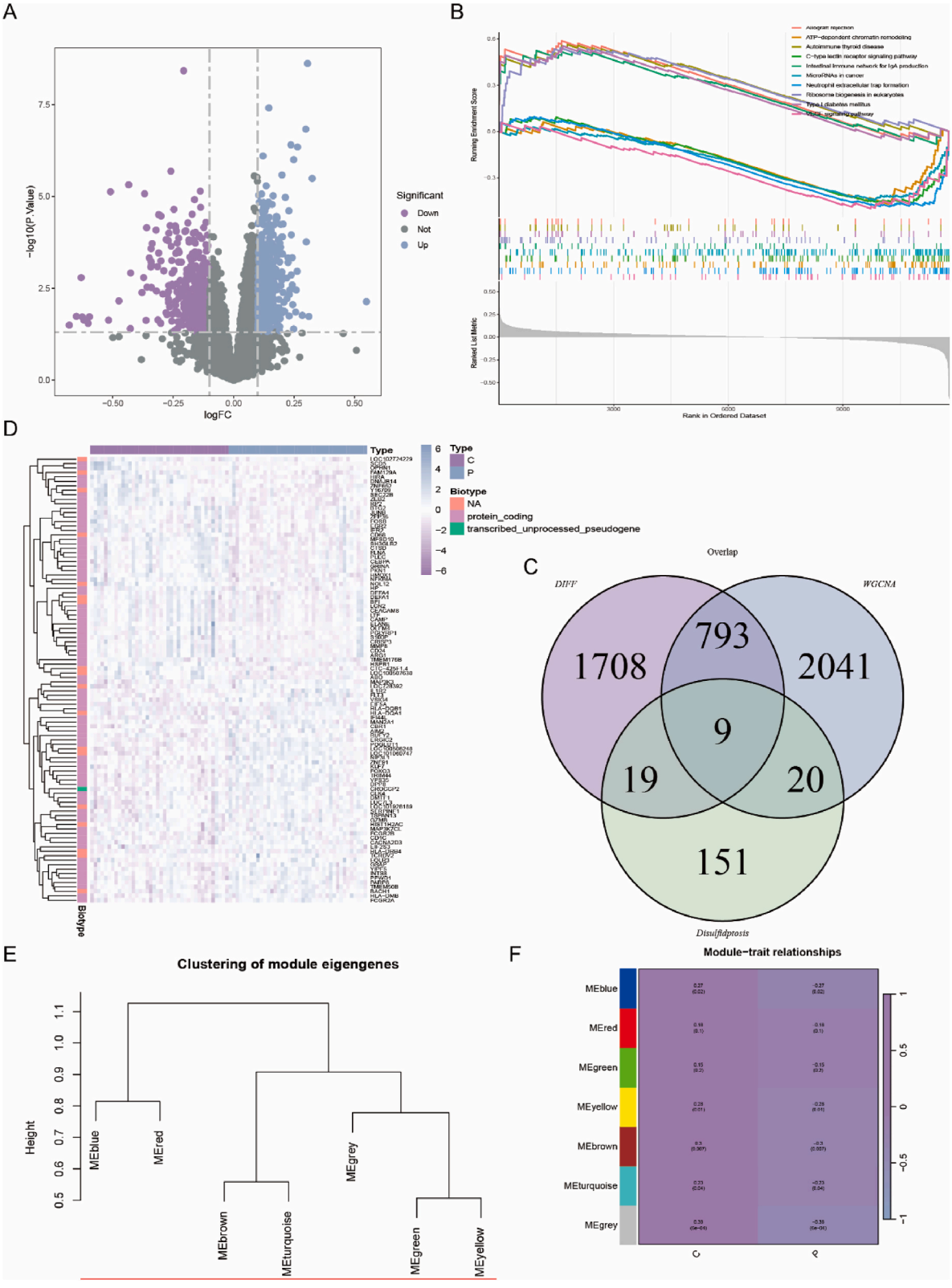

(caption on next page)

Fig. 1. Results of differential analysis and GSEA analysis and Identification of key genes; A: Volcano plot representation of differentially expressed genes; B: Pathway enrichment results for upregulated and downregulated genes in the differentially expressed gene set C: Venn diagram representation. D:Heatmap representation of differentially expressed genes, with blue indicating the normal group and yellow indicating the disease group; E: Visualization of different clusters in WGCNA; F: Module-trait relationship plot for different WGCNA clusters and clinical traits.

temperature. The sections were then incubated with a primary antibody against PGRMC2 (ab251875, 1:300, Abcam) at 4 °C overnight. Next, the sections were incubated with horseradish peroxidase-conjugated goat anti-rabbit secondary antibody for 1 h at 37 °C and counterstained with hematoxylin.

2.14. Sources of experimental samples

In our study, the collection of human blood samples and the acquisition of mouse tissues were key parts of the experiment. Firstly, human blood samples were obtained from six patients suffering from osteoporosis and six healthy controls. Their peripheral blood samples were collected and monocytes (monocytes) were isolated for subsequent experimental analysis. These blood samples were collected in strict compliance with ethical guidelines and all applicable legal requirements.

We divided C57BL/6 into 2 groups, the SHAM group and the OVX group, with 6 mice in each group. The mice were anaesthetised by intraperitoneal injection and lay supine, and the abdomen was depilated. Under aseptic conditions, the skin and muscle layers were cut at the level of the groin along the mid-abdominal line to expose the abdominal cavity. The uterus was separated and the ovaries were removed, the wounds were cleaned and the skin and basal layer were sutured in two layers. When the mice were awake, they were returned to clean cages and then put back to the rearing room for rearing, and the status and death of the mice were regularly observed and recorded. Three days after surgery, each mouse was injected with 40,000 units of penicillin daily to prevent infection. In the control group, only about 1 g of fat around the ovary was removed, while the ovary was retained, and the rest of the treatment was the same. 12W was taken, and the bone mineraldensity (BMD) of each group was measured by X-ray, then anaesthesia was injected intraperitoneally, and the blood was collected from the eyeballs and kept at room temperature for 2h, and then centrifuged at 3000r/min for 10min at 4 °C, and then the upper layer of the blood serum was separated and stored in the refrigerator at −80 °C for spare parts. Keep in the refrigerator at −80 °C for reserve. Mouse tibia specimens were taken for pathological testing.

3. Results

3.1. Differential analysis results and determination of key genes

We performed differential analysis on dataset GSE56815 and identified 2542 genes with p-values less than 0.05. We further plotted heatmaps (Fig. 1A) and volcano plots (Fig. 1D) for differentially expressed genes and performed GSEA analysis on upregulated genes. We found that upregulated gene sets were enriched in Allograft rejection, Autoimmune thyroid disease, Ribosome biogenesis in eukaryotes, etc. Downregulated gene sets were enriched in C-type lectin receptor signaling pathway, IL-17 signaling pathway, MicroRNAs in cancer, etc. (Fig. 1B).

Then We performed WGCNA analysis on the data. Fig. 1E shows that the data was divided into 7 clusters, and correlation analysis was performed as shown in Fig. 1F. We ultimately selected 5 modules with p-values less than 0.05 for subsequent analysis, totaling 2878 genes. Finally, we intersected differentially expressed genes, WGCNA module genes, and 200 selected thiosulfate death-related genes, ultimately identifying 9 key thiosulfate death-related genes for further analysis: IPO9, B2M, ACAP2, LONRF1, PGRMC2, CPM, MGAT2, XPOT, and UGDH (Fig. 1C).

3.2. Cluster analysis and machine learning screening results

Based on these key genes, we performed clustering on the data, dividing the data into two clusters, and separately displaying their PCA plot (Fig. 2A) and heatmap (Fig. 2B). In the ssGSEA analysis, we found significant differences in monocytes between the two clusters. In Gamma.delta.t.cell and Monocytes, significant differences were also found (Fig. 2C).

Further,we used LASSO to screen the aforementioned nine key genes, selecting six key genes (Fig. 2D and E). We then used Random Forest for screening, choosing the top six genes with the highest scores as key genes (Fig. 2G and H). We also used SVM for screening, selecting the top six genes with the highest scores as key genes (Fig. 2F and I).

3.3. Immune-related analysis

By taking the intersection of the key genes obtained from these three methods, we obtained four key genes for subsequent analysis: LONRF1, ACAP2, IPO9, and PGRMC2 (Fig. 3A).We conducted a correlation analysis between the screened key genes and immune infiltration results (Fig. 3B) and found that XPOT, PGRMC2, MGAT2, and ACAP2 are negatively correlated with Monocytes ($P < 0.05$). Further, we performed PPI analysis on the key genes screened by machine learning (Fig. 3C), showing their related protein-protein interactions. We individually plotted the correlation between the 4 key genes and immune cells; Fig. 3D shows the correlation between PGRMC2 and immune cells, it demonstrates a significant negative correlation between PGRMC2 and monocytes, as well as eosinophils and resting mast cells. Fig. 3E shows the correlation between LONRF1 and immune cells, Fig. 3F shows the correlation

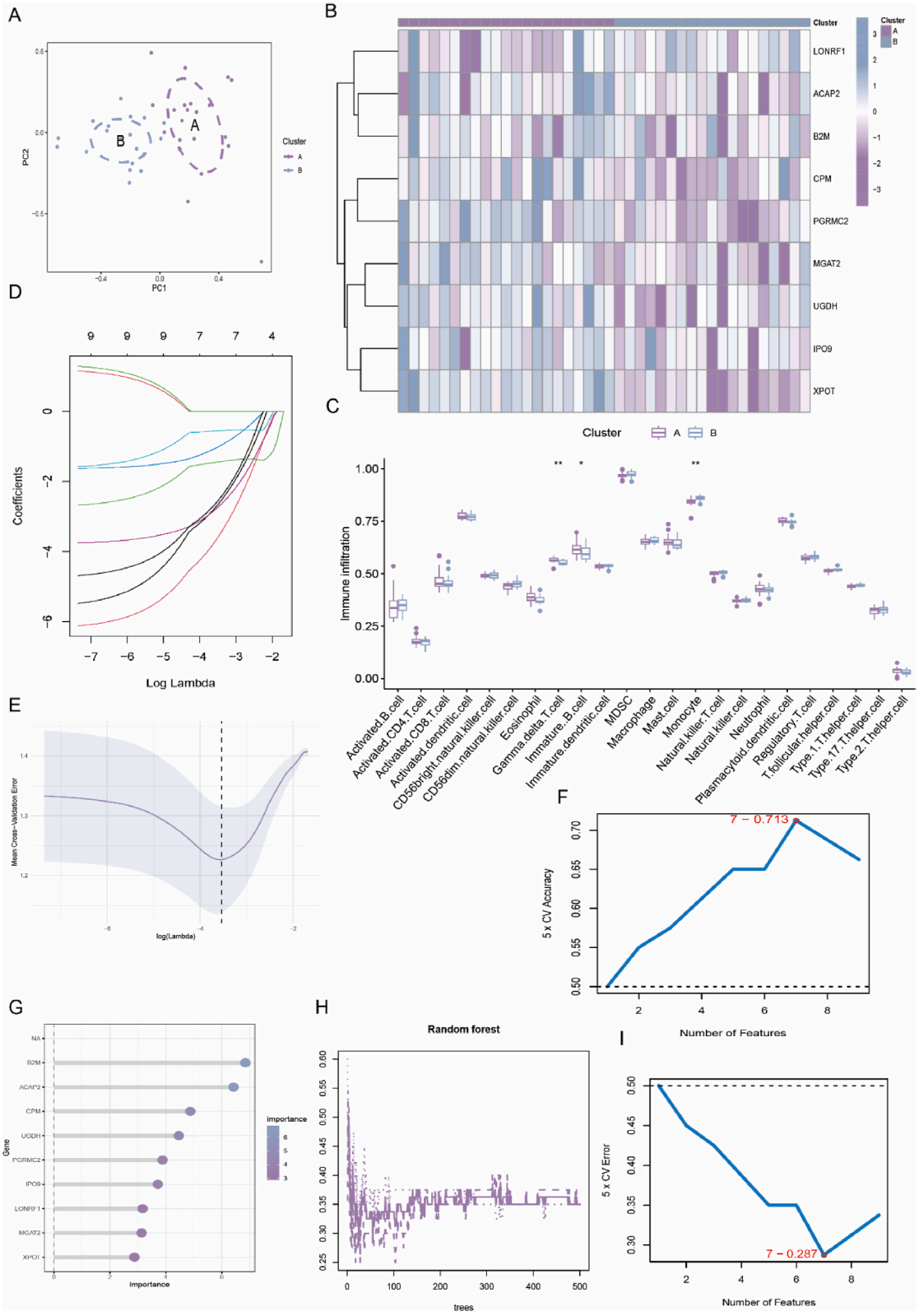

(caption on next page)

Fig. 2. Clustering analysis results and machine learning analysis results; A: 9 key genes divided the dataset into two clusters, A and B; B: Heatmap representation of the two clusters; C: Results of the ssgsea analysis, with blue representing cluster A and red representing cluster B. D–E: Lasso analysis fitting curves; G,H: Random forest analysis results visualization; F,I: SVM analysis results representation, with the highest point in D indicating accuracy and the lowest point in F indicating error rate.

between IPO5 and immune cells, and Fig. 3G shows the correlation between ACAP2 and immune cells.

3.4. Enrichment analysis and ROC analysis

We performed GSEA analysis on the four key genes. Fig. 4A shows the results for PGRMC2, mainly enriched in ALZHEIMERS_DISEASE, HUNTINGTONS_DISEASE, NEUROACTIVE_LIGAND_RECEPTOR_INTERACT; PARKINSONS_DISEASE, and SPLICEOSOME. Fig. 4B shows the results for ACAP2, mainly enriched in ASTHMA, NEUROACTIVE_LIGAND_RECEPTOR_INTERACTION, PRIMARY_IMMUNODEFICIENCY,RIBOSOME, and UBIQUITIN_MEDIATED_PROTEOLYSIS. Fig. 4C shows the results for IPO9, mainly enriched in CYTOKINE_CYTOKINE_RECEPTOR_INTERACTION, ECM_RECEPTOR_INTERACTION, and HYPERTROPHIC_CARDIOMYOPATHY_HCM. Fig. 4D shows the results for LONRF1, mainly enriched in AUTOIMMUNE_THYROID_DISEASE, NOD_LIKE_RECEPTOR_SIGNALING_PATHWAY, and OXIDATIVE_PHOSPHORYLATION. We further performed GSVA enrichment analysis on these four genes, and the results showed that the main enrichment in KEGG pathways included vesicle-mediated transport to the plasma membrane, steroid hormone-mediated signaling pathway, transition metal ion transport, and Neuroactive ligand-receptor interaction (Fig. 4F). Finally, we conducted ROC analysis on these four genes, with the highest AUC value for ACAP2 at 0.705, followed by IPO9 at 0.651, LONRF1 at 0.633, and PGRMC2 at 0.665. All four genes had AUC values greater than 0.6, confirming their close(Fig. 4E).

3.5. Single-cell analysis

We selected two single-cell datasets for analysis. Fig. 5A shows the distribution of various cells in normal bone tissue, and Fig. 5D shows the distribution of the key gene PGRMC2 in bone tissue. We can see that this gene is most abundant in ECs cells and more abundant in macrophages than in neutrophils, indicating that this gene promotes the transformation of monocytes to macrophages in bone tissue. Furthermore, Fig. 5B shows the single-cell distribution in PMOP disease samples, and Fig. 5E and F shows the distribution of the key gene PGRMC2 in various cells. We found that it is most abundant in BM-MSC cells. Further, we extracted this cluster of cells for further annotation analysis, as shown in Fig. 5C, dividing the cells into four clusters: Osteogenic, Terminal, Adipogenic, and Chondrogenic. We analyzed the content of the key gene in each cell and found that PGRMC2 is most abundant in the Osteogenic cluster.

3.6. Correlation analysis results and Mendelian randomization analysis

We conducted a correlation analysis between PGRMC2 and various genes in the microarray-based assay dataset. The results showed a positive correlation between PGRMC2 and SMARCA5 with $r = 0.53$, $p < 0.01$ (Fig. 6A and B), a positive correlation between PGRMC2 and ZNF146 with $r = 0.63$, $p < 0.01$ (Fig. 6C), a negative correlation between PGRMC2 and ZNF384 with $r = -0.55$, $p < 0.01$ (Fig. 6D), a positive correlation between PGRMC2 and CHD1 with $r = 0.52$, $p < 0.01$ (Fig. 6E), and a negative correlation between PGRMC2 and CREB3L1 with $r = -0.52$, $p < 0.01$ (Fig. 6F). Fig. 6G shows the results of the ceRNA network analysis for the key genes.

Then Fig. 6H is a forest plot of the Mendelian randomization analysis, displaying the results of three different Mendelian randomization methods (MR Egger, weighted median, and inverse variance weighted) applied to the effect of PGRMC2 on osteoporosis. From the results, we can see that the inverse variance weighted method shows a significant effect of PGRMC2 on osteoporosis ($p = 0.0048$), and the effect size is less than 1 ($OR = 0.6836$), suggesting that PGRMC2 may be associated with a reduced risk of osteoporosis. Fig. 6I is a funnel plot, typically used to inspect the bias and heterogeneity of the Mendelian randomization analysis. In an ideal situation without bias and heterogeneity, the points in the plot should be evenly distributed on both sides of the central line, forming an inverted funnel shape. Fig. 6J is a scatter plot, showing the effect sizes and precision of each SNP. This plot can help us understand the size and direction of the impact of each SNP on the outcome, as well as their contribution to the overall results. Each point represents an SNP, with the size of the point typically representing its weight (for example, sample size or statistical power), the horizontal position indicating its effect on the exposure variable (here is PGRMC2), and the vertical position indicating its effect on the outcome variable (here is osteoporosis).

3.7. qRT-PCR validation of key genes

We selected monocytes from postmenopausal osteoporosis patients and healthy individuals for qRT-PCR analysis. In our results, we found that PGRMC2 exhibited significant differences ($P < 0.05$), while the other three genes showed no significant differences. Fig. 7A shows the results for IPO9 ($P > 0.05$), Fig. 7B for ACAP2 ($P > 0.05$), Fig. 7C for PGRMC2 ($P < 0.05$), and Fig. 7D for LONRF1 ($P > 0.05$).

3.8. The expression of PGRMC2 was reduced in OVX mice

We demonstrated decreased expression of PGRMC2 in OVX mice by protein immunoblotting (Fig. 7E). Similarly, our

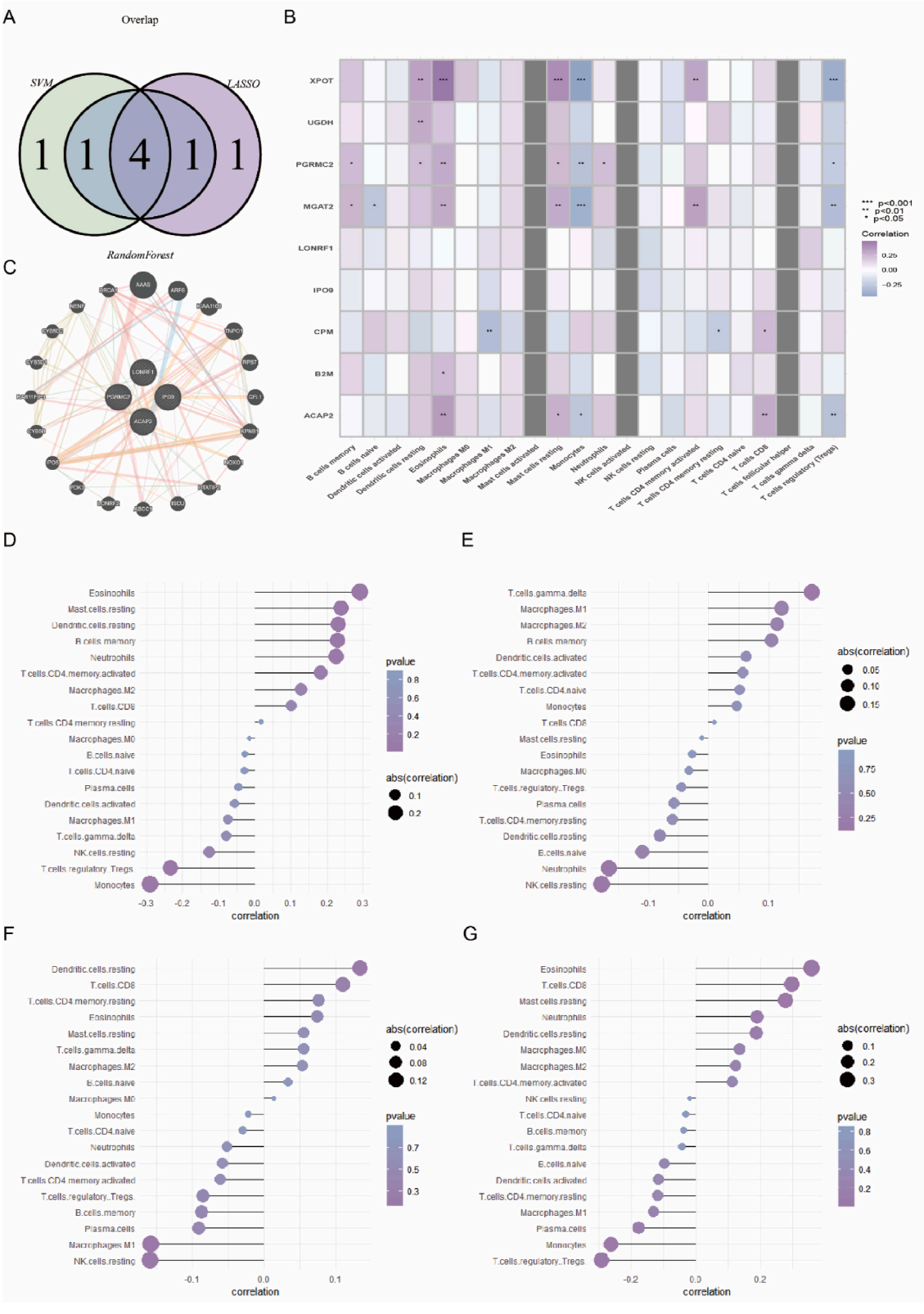

(caption on next page)

Fig. 3. Immune analysis results; A: Venn diagram intersection results for the three types of machine learning analyses. B: Heatmap representation of the correlation analysis between the 9 key genes and immune infiltration analysis results; C: Protein-protein interaction network for 4 key genes; D: Correlation between PGRMC2 and immune cells; E: Correlation between LONRF1 and immune cells; F: Correlation between IPO5 and immune cells; G: Correlation between ACAP2 and immune cells.

immunohistochemical assay revealed that PGRMC2 expression was reduced in OVX mice (Fig. 7F and G).

4. Discussion

In the past decade, advances in scRNA-seq technology have had a transformative impact on biomedical research, enabling single-cell transcriptome analysis and characterization at unprecedented resolution and throughput. In addition, scRNA-seq technology helps identify new or rare cell types. Applying single-cell data analysis to in-depth exploration of diseases helps understand the mechanisms of disease development [35]. Disulfidptosis, as the latest cell death mechanism, is related to the formation and breaking of protein disulfidptosis bonds in disease development. In some cases, disordered disulfidptosis bond formation may lead to cell death. In PMOP, it is the imbalance of differentiation between osteoclasts and osteoblasts that leads to PMOP formation, which is closely related to cell death. In the endometrium, PGRMC2 expression variations are closely related to cell proliferation and differentiation [36]. Similarly, in bone tissue, the activity of osteoblasts and osteoclasts is regulated by a complex network of endocrine signals and cytokines. We hypothesize that PGRMC2 may influence the differentiation and activity of these cells, potentially affecting the bone remodeling process. Additionally, responses in endometrial cells suggest that PGRMC2 is involved in managing cellular stress and endoplasmic reticulum stress. Bone cells also face similar pressures, especially in environments of bone remodeling and metabolic stress. We speculate that if there are problems with the formation or repair of disulfidptosis bonds in bone-related proteins, this may affect bone density and fracture risk, leading to the development of osteoporosis.

In our study, we identified nine key genes through the analysis of differentially expressed genes, WGCNA key module genes, and disulfidptosis-related genes, including IPO9, B2M, ACAP2, LONRF1, PGRMC2, CPM, MGAT2, XPOT, and UGDH. The dataset used for the transcriptome analysis of patients' peripheral blood mononuclear cells. We classified the dataset into two clusters using these nine genes and found significant differences in Monocytes through ssGSEA analysis, further validating our conclusions. This indicates that these disulfidptosis genes have a close relationship with monocytes. To further screen key genes in the disease process, we used three machine learning methods for screening and ultimately identified four key genes: LONRF1, ACAP2, IPO9, and PGRMC2. Regarding the analysis of the correlation between PGRMC2 and immune cells, we shows a significant negative correlation between PGRMC2 and monocytes, eosinophils, and resting mast cells. These findings suggest that PGRMC2 may have a certain inhibitory role in immune regulation, which could be achieved by modulating the activity and function of these cells. Specifically, the reduction in monocytes may weaken their function as precursors to osteoclasts in bone remodeling, while the decreased correlation with eosinophils and mast cells may reflect PGRMC2's potential role in regulating immune responses. This analysis reveals the possible role of PGRMC2 in regulating immune cells, especially in the bone microenvironment, providing a basis for further functional research. In previous studies, it was found that the LONRF protein family consists of three isoenzymes, LONRF1-3, and Lonrf1 is ubiquitously expressed in various tissues. Its expression in LSEC and Kupffer cells increases with liver aging. LONRF1 may play a critical role in linking oxidative damage response and tissue remodeling in different modes of wound healing in aging and non-aging cells [37]. ACAP2 is recruited to the peripheral tubular membrane, where it activates Arf6 to allow membrane recycling back to the plasma membrane, playing a role in the cell periphery. It has a certain relationship with exosomes. Previous studies have found that ACAP2 downregulation triggered by exosome-derived miR-3656 further promotes the activation of PI3K/AKT and β-catenin signaling pathways, ultimately improving the growth of ESCC cells in vitro and in xenograft models [38]. Previous research on IPO9 has found associations with apoptosis and cancer metastasis [39],and it has been found that downregulation of IPO9 expression is associated with a significant decrease in apoptotic cell populations and a decrease in F-actin content in whole cells as well as cortical and nuclear/perinuclear regions [40]. In subsequent qRT-PCR analysis, PGRMC2 showed significant differences between the experimental and control groups. Current research has not reported its association with PMOP. We believe that this gene can be used as a diagnostic predictor for PMOP. Previous studies have found that regulation of PGRMC2 may restore obesity-related defects in adipocytes, and it is closely related to adipocytes [41]. t is worth noting that most of the research on this gene is related to female hormones. Clark found that Pgrmc2 is essential for maintaining uterine tissue structure and normal female reproductive lifespan, and conditional ablation of progesterone receptor membrane component 2 causes female premature reproductive senescence. This gene can cause premature ovarian failure in women [42]. On the other hand, the occurrence and development of PMOP are closely related to female hormones, so we believe that this gene can affect the occurrence and development of PMOP by affecting hormone secretion. Moreover, there is a positive correlation between PGRMC2 and ZNF146. We hypothesize that these two genes may jointly influence the occurrence and development of PMOP through synergistic effects. To gain a deeper understanding of the mechanism of PGRMC2 in PMOP, we combined single-cell data for analysis. We found that in bone tissue, the gene is more distributed in macrophages than in monocytes [43]. Previous studies have found that macrophages play an important role in osteoporosis, and macrophage polarization may help promote osteoblast differentiation, enhance bone formation and mineralization processes, and activated macrophages may secrete pro-inflammatory cytokines, which can cause bone loss by inducing osteoclastogenesis and are associated with the activation of bone resorption [44]. Therefore, we speculate that PGRMC2 promotes the differentiation of monocytes into macrophages in bone tissue, thereby affecting the development of PMOP. Further, we analyzed the scRNA-seq data in PMOP and found that PGRMC2 is mainly distributed in BM-MSCs. Bone marrow mesenchymal stem cells (BM-MSCs) play a key role in bone metabolism, bone homeostasis, and bone repair, but their regenerative

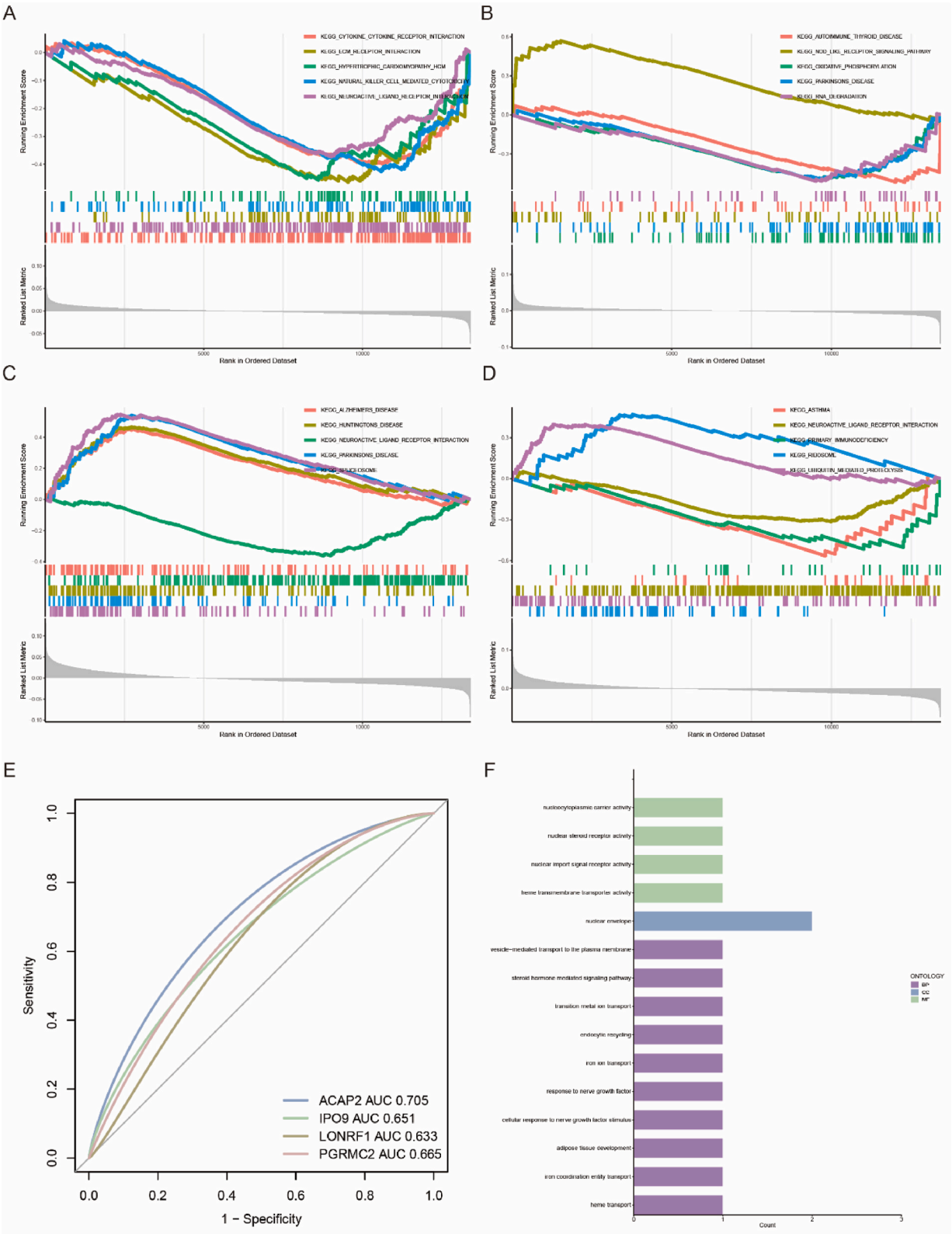

Fig. 4. Enrichment analysis and ROC analysis results; A: GSEA analysis results for PGRMC2; B: GSEA analysis results for ACAP2; C: GSEA analysis results for IPO9; D: GSEA analysis results for LONRF1; E: ROC curve results for the 4 key genes; F: GO and KEGG enrichment results for the key genes.

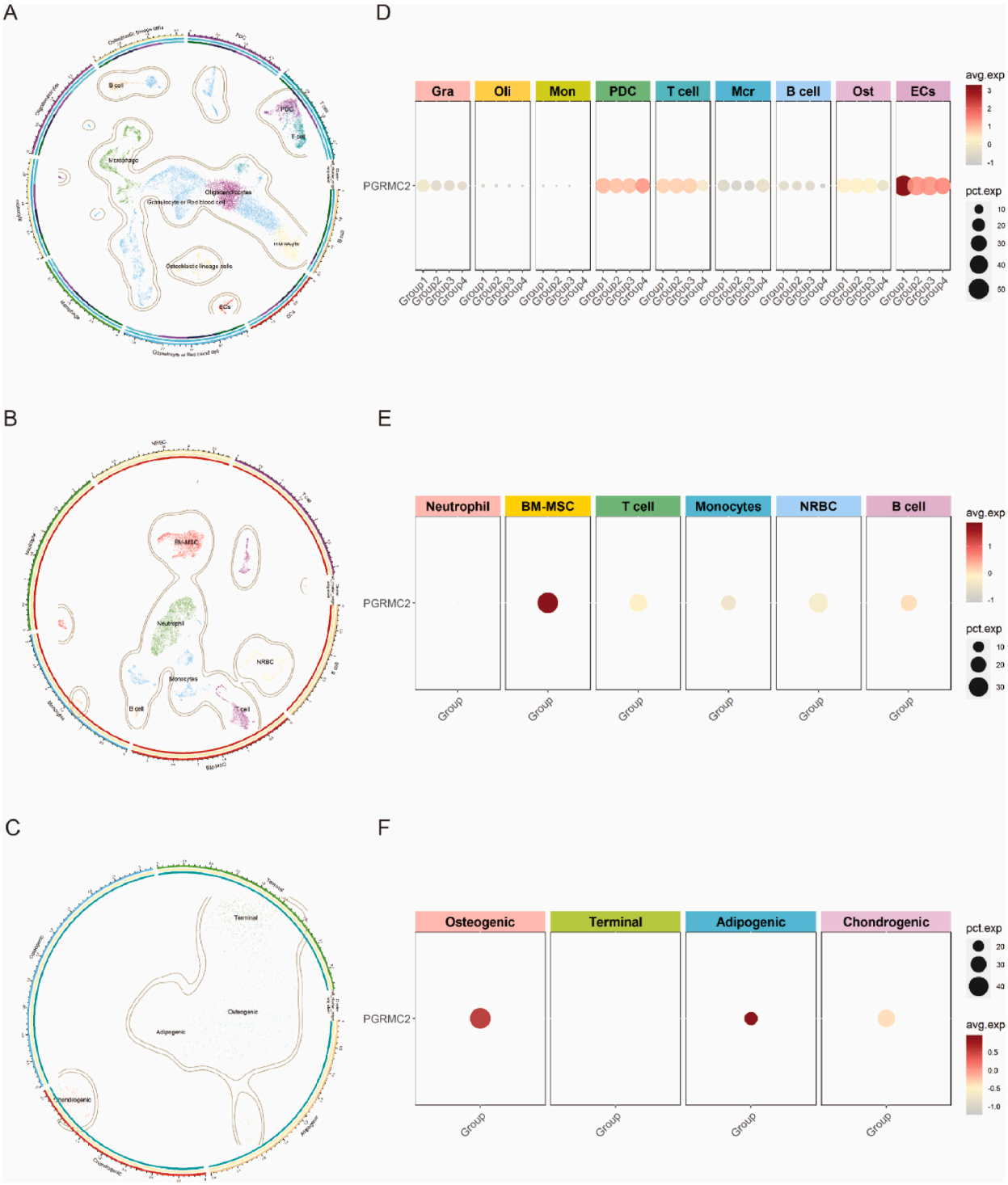

Fig. 5. Single-cell analysis results; A: Single-cell annotation results for GSE169396; B: Single-cell annotation results for GSE147287; C: Further annotation results for BM-MSC in GSE147287; D: PGRMC2 distribution results in GSE169396; E: PGRMC2 distribution results in GSE147287; F: PGRMC2 distribution results in BM-MSC.

capacity may be weakened in postmenopausal osteoporosis patients [45]. Further annotation of the BM-MSC cell clusters revealed osteoblasts, chondrocytes, and adipocytes, among others. We found that PGRMC2 is more abundant in osteoblasts and adipocytes. Previous studies have found that bone marrow adipocytes (BMAds) accumulate in various osteoporotic conditions and interfere with

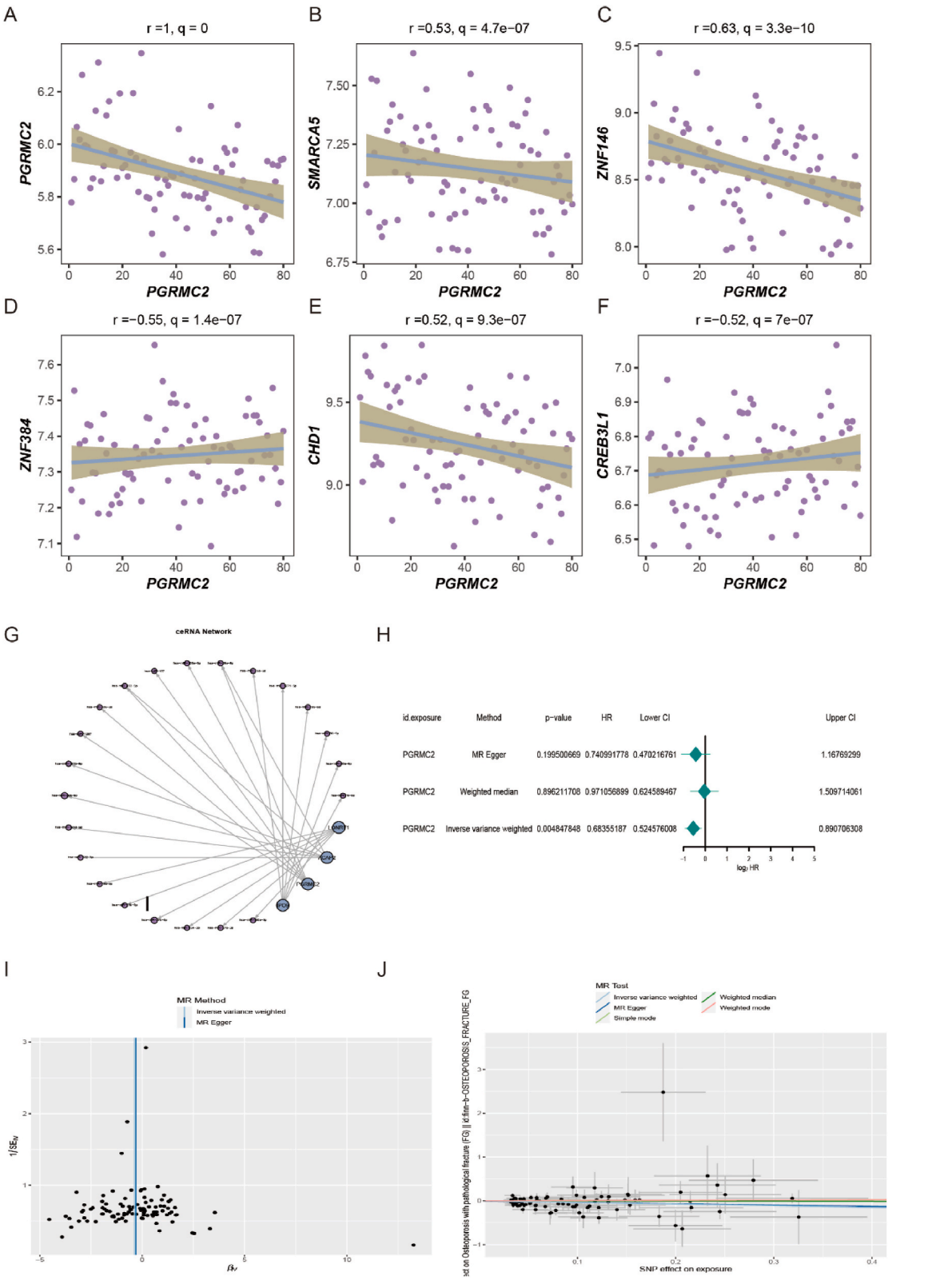

(caption on next page)

Fig. 6. Correlation analysis of PGRMC2 and Results of Mendelian Randomization Analysis. A: Correlation analysis between PGRMC2 and PGRMC2; B: Correlation analysis between PGRMC2 and SMARCA5; C: Correlation analysis between PGRMC2 and ZNF146; D: Correlation analysis between PGRMC2 and ZNF384; E: Correlation analysis between PGRMC2 and CHD1; F: Correlation analysis between PGRMC2 and CREB3L1.G:ceRNA Network for hub genes. The yellow color represents the four key genes, and the pink color represents the predicted miRNAs. H: Forest plot, presenting the estimated effect of PGRMC2 on osteoporosis and its 95 % confidence interval. The three horizontal lines represent the results of three methods: MR Egger, Weighted Median, and Inverse Variance Weighted. I: Funnel plot, used to evaluate the bias and heterogeneity of the Mendelian randomization analysis. J: Scatter plot, showing the effects of each SNP on the exposure variable (PGRMC2) and the outcome variable (osteoporosis). Each point represents an SNP, with its position indicating the size and direction of the effect, and its size representing the weight.

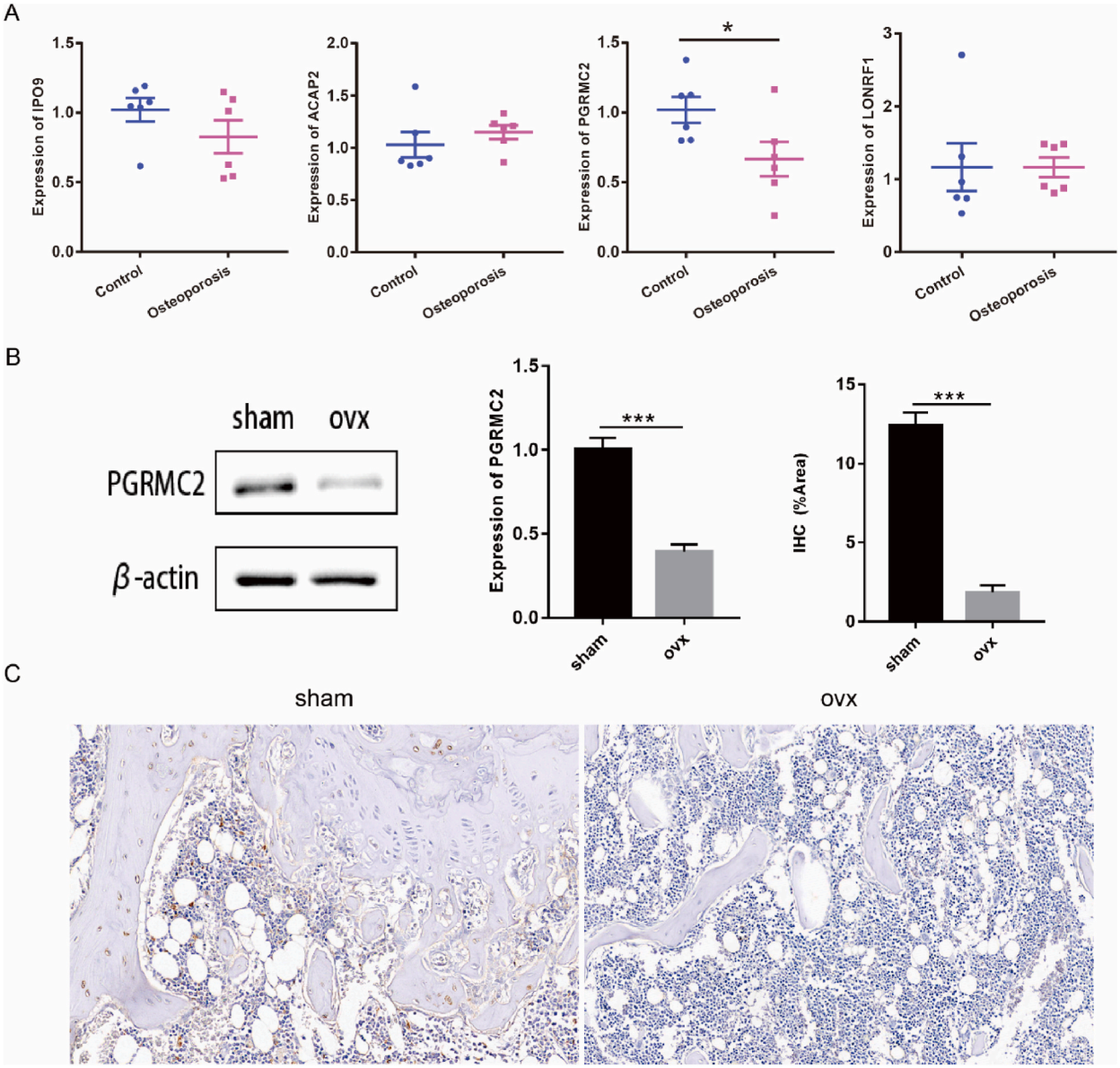

Fig. 7. qRT-PCR results; A: IPO9 results representation; B: ACAP2 results representation; C: PGRMC2 results representation; D: LONRF1 results representation; E: The expression of PGRMC2 was detected by Western blot in sham mice and OVX mice; F, G: Detection and quantification of PGRMC2 by immunohistochemistry.

bone remodeling by secreting various factors. Additionally, the extracellular matrix (ECM) produced by bone marrow adipocytes can have a detrimental effect on the osteoblastic differentiation of bone marrow mesenchymal stem cells (BM-MSCs) [46]. PGRMC2's role in osteocytes involves interactions among various cells within the basic multicellular unit (BMU). Studies have shown that osteocytes, osteoblasts, osteoclasts, bone lining cells, osteomacs, and endothelial cells communicate and coordinate closely during bone

remodeling through complex autocrine and paracrine mechanisms [47]. These cells regulate bone remodeling through cell signaling networks and receptor-ligand complexes, with osteocytes acting in the bone microenvironment by secreting and membrane-bound factors. Additionally, osteomacs interweave with other bone lining cells on the bone surface, regulating osteoblast function and playing an important role in bone formation and mineralization. Endothelial cells in the bone microenvironment regulate local endothelial cells and pericytes through the expression and function of angiogenic factors, which are crucial for bone growth and remodeling [48]. In summary, PGRMC2 may play an important role in osteocyte function and bone remodeling by regulating the interactions of these cells within the BMU. We speculate that PGRMC2 affects BM-MSCs by influencing osteogenic and adipogenic differentiation, thereby impacting the development of PMOP. At the same time, this study also has some limitations. While the paper utilizes single-cell data to analyze the distribution and role of PGRMC2 in PMOP, these results require further experimental validation to confirm their importance in the development and progression of PMOP. In the study, qRT-PCR was used to validate four key genes, but only PGRMC2 showed significant differences between the experimental and control groups. The expression of PGRMC2 was detected by Western blot in sham mice and OVX mice. However, the function and role of the other genes still require further investigation.

Ethics approval and consent to participate

This study was approved by the Research Ethics Committee of Lanzhou University Second Hospital (Approval No. 2023A-796) and conducted in accordance with the Declaration of Helsinki. we confirm that informed consent was obtained from all subjects and/or their legal guardian(s). All animal experiments were approved by the Animal Experiment Management Committee of Lanzhou University Second Hospital (Approval No.D2023-491).

Consent for publication

Not applicable.

Ethical guidelines

The study protocol adheres to the principles set forth by the 1964 Declaration of Helsinki and its later amendments.

Availability of data and materials

The datasets during and/or analyzed during the current study available from the corresponding author on reasonable request.

Funding

This study was supported by the National Natural Science Foundation of China (81960403, 82060405 and 82360436); Lanzhou Science and Technology Plan Program (2021-RC-102); Natural Science Foundation of Gansu Province (22JR5RA943, 22JR5RA956 and 23JRRA1500); Cuiying Scientific and Technological Innovation Program of Lanzhou University Second Hospital (CY2021-MS-A07, CY2022-MS-A19); Gansu Provincial Department of Education: Outstanding Graduate Student "Innovation Star" Project (2023CXZX-157).

Data availability statement

Availability of data and materials: The datasets during and/or analyzed during the current study are available from the corresponding author on reasonable request. Sharing research data helps other researchers evaluate your findings, build on your work, and increase trust in your article. We encourage all our authors to make as much of their data publicly available as reasonably possible. The data associated with this study have not been deposited into a publicly available repository. The data will be made available on request.

All data used in this study are publicly available and were retrieved from the Gene Expression Omnibus (GEO) database, which is hosted by the National Center for Biotechnology Information (NCBI). The data can be accessed via the following link: https://www.ncbi.nlm.nih.gov/geo/. This ensures transparency and reproducibility of our findings, as other researchers can readily access and verify the dataset used in our analyses. Specific accession numbers and details regarding the datasets utilized will be provided within the manuscript to facilitate easy access for peer verification and further studies.

CRediT authorship contribution statement

Yaobin Wang: Writing – original draft, Software, Methodology, Investigation, Formal analysis, Conceptualization. **Hefang Xiao:** Writing – original draft, Software, Methodology, Investigation, Formal analysis, Conceptualization. **Yi Chen:** Writing – original draft, Data curation. **Xiaoyun Sheng:** Writing – original draft, Data curation. **Zhiwei Feng:** Visualization, Investigation. **Bo Peng:** Supervision, Resources. **Zhongcheng Liu:** Supervision, Resources. **Hongwei Zhan:** Validation, Software. **Dejian Xiang:** Writing – review & editing, Visualization. **Chengjun Zhang:** Writing – review & editing, Visualization. **Yayi Xia:** Writing – review & editing, Supervision,

Resources, Funding acquisition, Conceptualization. **Bin Geng:** Writing – review & editing, Supervision, Resources, Funding acquisition, Conceptualization.

Declaration of competing interest

The authors declare that they have no known competing financial interests or personal relationships that could have appeared to influence the work reported in this paper.

References

[1] V. Fischer, M. Haffner-Luntzer, Interaction between bone and immune cells: implications for postmenopausal osteoporosis, in: Seminars in Cell & Developmental Biology, Elsevier, 2022.
[2] L.J. Melton, 3rd, How many women have osteoporosis now? J. Bone Miner. Res. 10 (2) (1995) 175–177.
[3] D.S. Anupama, et al., Burden of osteopenia and osteoporosis among postmenopausal women in India: a systematic review and meta-analysis, J Midlife Health 13 (2) (2022) 107–114.
[4] K.T. DeSapri, R. Brook, To scan or not to scan? DXA in postmenopausal women 87 (4) (2020) 205–210.
[5] A. Sinno, et al., Hormone therapy (HT) in women with gynecologic cancers and in women at high risk for developing a gynecologic cancer: a Society of Gynecologic Oncology (SGO) clinical practice statement: this practice statement has been endorsed by the North American, Menopause Society 157 (2) (2020) 303–306.
[6] R.A. Lobo, A.J.T.L.D. Gompel, Endocrinology, Management of Menopause: a View towards Prevention, 2022.
[7] Y. Zhang, et al., Single-cell RNA Sequencing in Cancer Research, vol. 40, 2021, pp. 1–17.
[8] R. Nayak, Y.J.G. Hasija, A hitchhiker's guide to single-cell transcriptomics and data analysis pipelines 113 (2) (2021) 606–619.
[9] K. Zhu, et al., Single-cell analysis reveals the pan-cancer invasiveness-associated transition of adipose-derived stromal cells into COL11A1-expressing cancer-associated fibroblasts, PLoS Comput. Biol. 17 (7) (2021) e1009228.
[10] X. Liu, et al., Actin cytoskeleton vulnerability to disulfide stress mediates disulfidptosis, Nat. Cell Biol. 25 (3) (2023) 404–414.
[11] t. wang, et al., Disulfidptosis Classification of Hepatocellular Carcinoma Reveals Correlation with Clinical Prognosis and Immune Profile, 2023.
[12] T. Barrett, et al., NCBI GEO: archive for functional genomics data sets—update 41 (D1) (2012) D991–D995.
[13] G.K.J.B. Smyth, Limma: linear models for microarray data. c.b.s.u. R, and Bioconductor, 2005, pp. 397–420.
[14] P. Langfelder, S.J.B.b. Horvath, WGCNA: an R package for weighted correlation network analysis 9 (1) (2008) 1–13.
[15] P.S. Russo, et al., CEMiTool: a Bioconductor package for performing comprehensive modular co-expression analyses 19 (1) (2018) 1–13.
[16] M. Yi, et al., ssGSEA score-based Ras dependency indexes derived from gene expression data reveal potential Ras addiction mechanisms with possible clinical implications 10 (1) (2020) 1–16.
[17] J. Friedman, et al., Package 'glmnet', 2021.
[18] S. RcolorBrewer, M.A.J.U.o.C. Liaw, Berkeley: Berkeley, CA, USA, Package 'randomforest', 2018.
[19] Z. Wang, A. Brenner, An integrated method for forest canopy cover mapping using Landsat ETM+ imagery, in: ASPRS/MAPPS Conference, 2009. Texas, USA.
[20] B. Chen, et al., Profiling Tumor Infiltrating Immune Cells with CIBERSORT, 2018, pp. 243–259.
[21] Z. Lü, W.J.C. Huang, O. Research, PERM for solving circle packing problem 35 (5) (2008) 1742–1755.
[22] K. Hu, Become competent in generating RNA-seq heat maps in one day for novices without prior R experience. Nuclear Reprogramming: Methods and Protocols, 2021, pp. 269–303.
[23] R. Kolde, M.R.J.R.p. Kolde, Package 'pheatmap' 1 (10) (2018).
[24] L. Wang, et al., Cuproptosis related genes associated with Jab1 shapes tumor microenvironment and pharmacological profile in nasopharyngeal carcinoma, Front. Immunol. 13 (2022) 989286.
[25] T. Wei, et al., Package 'corrplot' 56 (316) (2017) e24.
[26] L. Wilkinson, ggplot2: Elegant Graphics for Data Analysis by WICKHAM, H, Oxford University Press, 2011.
[27] H. Wickham, W. Chang, M.H.J.C.e.d.v.u.t.g.o.g.V. Wickham, Package 'ggplot2' 2 (1) (2016) 1–189.
[28] X. Robin, et al., pROC: an open-source package for R and S+ to analyze and compare ROC curves, BMC Bioinf. 12 (2011) 1–8.
[29] X. Robin, et al.. Package 'pROC', Technical Report, 2017. Available online: https://cran.r-project.org/web.
[30] S. Hänzelmann, R. Castelo, J.J.B.b. Guinney, GSVA: Gene Set Variation Analysis for Microarray and RNA-Seq Data, vol. 14, 2013, pp. 1–15.
[31] A. Gribov, et al., SEURAT: Visual Analytics for the Integrated Analysis of Microarray Data, vol. 3, 2010, pp. 1–6.
[32] A.J.P.o. Platzer, Visualization of SNPs with t-SNE 8 (2) (2013) e56883.
[33] Q. Xu, et al., Single-cell RNA transcriptome reveals the intra-tumoral heterogeneity and regulators underlying tumor progression in metastatic pancreatic ductal adenocarcinoma 7 (1) (2021) 331.
[34] I.M. Mackay, K.E. Arden, A.J.N.a.r. Nitsche, Real-time PCR in virology 30 (6) (2002) 1292–1305.
[35] C.M. Stein, et al., Single-cell omics: overview, analysis, and application in biomedical, science 122 (11) (2021) 1571–1578.
[36] Y. Medina-Laver, et al., Deciphering the role of PGRMC2 in the human endometrium during the menstrual cycle and in vitro decidualization using an in vitro approach, Hum. Reprod. 39 (5) (2024) 1042–1056.
[37] D. Li, et al., Transcriptomic Characterization of Lonrf1 at the Single-Cell Level under Pathophysiological Conditions, 2023, p. mvad021.
[38] Y. Jin, et al., Cancer-associated fibroblasts-derived exosomal miR-3656 promotes the development and progression of esophageal squamous cell carcinoma via the ACAP2/PI3K-AKT signaling pathway 17 (14) (2021) 3689.
[39] K. Fujii, et al., Differential proteomic analysis between small cell lung carcinoma (SCLC) and pulmonary carcinoid tumors reveals molecular signatures for malignancy in lung cancer 12 (6) (2018) 1800015.
[40] M. Izdebska, et al., Downregulation of importin-9 protects MCF-7 cells against apoptosis induced by the combination of garlic-derived alliin and paclitaxel 35 (5) (2016) 3084–3093.
[41] A. Galmozzi, et al., PGRMC2 is an intracellular haem chaperone critical for adipocyte function 576 (7785) (2019) 138–142.
[42] N.C. Clark, et al., Conditional ablation of progesterone receptor membrane component 2 causes female premature reproductive senescence 158 (3) (2017) 640–651.
[43] J. Muñoz, et al., Macrophage polarization and osteoporosis: a review, Nutrients 12 (10) (2020).
[44] D.H. Yang, M.Y. Yang, The role of macrophage in the pathogenesis of osteoporosis, Int. J. Mol. Sci. 20 (9) (2019).
[45] A. Saito, et al., Umbilical cord extracts improve osteoporotic abnormalities of bone marrow-derived mesenchymal stem cells and promote their therapeutic effects on ovariectomised rats, Sci. Rep. 8 (1) (2018) 1161.
[46] L. Entz, et al., The extracellular matrix of human bone marrow adipocytes and glucose concentration differentially alter mineralization quality without impairing osteoblastogenesis, Bone Rep 17 (2022) 101622.
[47] J. Kular, et al., An overview of the regulation of bone remodelling at the cellular level 45 (12) (2012) 863–873.
[48] K. Chen, et al., Communications between bone marrow macrophages and bone cells in bone remodeling, Front. Cell Dev. Biol. 8 (2020) 598263.